King Saud University

Arabian Journal of Chemistry

www.ksu.edu.sa
www.sciencedirect.com

ORIGINAL ARTICLE

Immobilized sulfonic acid functionalized ionic liquid on magnetic cellulose as a novel catalyst for the synthesis of triazolo[4,3-*a*]pyrimidines

Azar Jahanbakhshi, Mahnaz Farahi

Department of Chemistry, Yasouj University, P. O. Box 353, Yasouj 75918-74831, Iran

Abstract   The Brønsted acidic ionic liquid 1-(propyl-3-sulfonate) vinyl imidazolium hydrogen sulfate [IL] was supported on modified magnetic cellulose. The physical structure, composition, and functional groups of the novel supported ionic liquid catalyst were characterized via XRD, FT-IR, EDS, SEM, VSM, TGA, TEM, and BET techniques. Owing to the combination of nano-support features and flexible imidazolium linkers, it acted as a "quasi-homogeneous" catalyst to catalyze the preparation of triazolo[4,3-*a*]pyrimidine derivatives by a one-pot three-component reaction of active methylene compounds (ethyl cyanoacetate or malononitrile), aminotriazole and aryl aldehydes. The catalyst shows good catalytic activity for the synthesis of triazolo pyrimidines after six times of recycling.

© 2022 The Authors. Published by Elsevier B.V. on behalf of King Saud University. This is an open access article under the CC BY-NC-ND license (http://creativecommons.org/licenses/by-nc-nd/4.0/).

1. Introduction

From significant important aspects of green chemistry are the expansion and usage of green solvents. Nowadays, ILs is introduced as green solvents in alternative to conventional volatile organic solvents. ILs, liquid salts, were formed wholly of cations and anions and are mainly defined as being liquid beneath an ideal amount, such as 100 °C or at room temperature (Morais et al., 2022; Minea and Sohel Murshed, 2021; Greer et al., 2020). Ionic liquids (ILs) as eco-friendly reaction media have attracted increasing attention due to their particular properties, such as tunable acidity, selective dissolvability, very low viscos-

ity, negligible vapor pressure, wide liquid range, high thermal stability, and easiness of product separation (Han et al., 2022; Singh and Savoy, 2020; Tajbakhsh et al., 2013; Miao et al., 2011a, 2011b). The strongly acidic ionic liquids (Brønsted-type and Lewis-type) have been exploited as efficient catalysts for many reactions and generally can afford reusability, higher yields, and selectivity against traditional acid catalysts (Azizi and Shirdel, 2016; Cole et al., 2002; Tayebee et al., 2015). Among them, SO₃H-functionalized ILs with a hydrogen sulfate counteranion have been intensively studied as a class of dual acidic functionalized ILs during the last years since the existence of both SO₃H-functional groups and the hydrogen sulfate counteranion can increase their acidities. Ionic liquids based on imidazolium cation, because of their high stability, are also widely used in organic reactions in laboratories and industries (Tayebee et al., 2017; Elavarasan et al., 2020; Miao et al., 2011a, 2011b). However, immobilizing ionic liquids on various solid supports is one of the efficient ways to overcome these problems. An exciting combining feature of ionic liquid with those of supporting material will develop novel performances when the

Production and hosting by Elsevier

synergistic effects appear (Li et al., 2014a, 2014b). Therefore, stabilized ionic liquid phase catalyst is an emerging concept in heterogeneous catalysis. Mainly, polymer-supported ionic liquids facilitate easy catalyst recovery, high selectivity, recyclability, and less contamination of products with a catalyst (Patil et al., 2022; Pei et al., 2022). The heterogeneous catalysts, due to easy segregation from the products, recyclability and reusability, and much stability, received remarkable attention (Saeedi and Rahmati, 2022). The heterogenization of ILs on appropriate porous carriers (Oliveira et al., 2019; Sun et al., 2017; Wang et al., 2020), suitable magnetic nanoparticles (Veisi et al., 2021; Zolfigol et al., 2016; Sheykhan et al., 2011; Zhang et al., 2012a, 2012b), immobilized on solid supports by either a physical coating of ionic liquids on Al_2O_3 (Li et al., 2017; Khoshnevis et al., 2013), SiO_2 (Jamshidi et al., 2018; Testa et al., 2010; Niknam et al., 2011) and TiO_2 (Atghia and Sarvi-Beigbaghlou, 2013; Tabrizian et al., 2016) or covalent attachment of ionic liquids to the support surface, would be a viable and appealing approach to fabricate an efficient solid catalyst with superior activity and stability (Safari and Ahmadzadeh, 2017). In this sense, cellulose, one of the most critical natural organic polymers, can be used as nanocomposite, support materials, and emulsions because of various advantages such as biocompatible, renewability, flexibility, dimensional stability, and ability to modify its surface chemistry and hydrophilicity (Kamel and Khattab, 2021; Hamdy et al., 2017; Sabaqian et al., 2017; Abdelhameed et al., 2020). The hydroxyl groups are reactive on the surface of cellulose, which helps to modify their surface with organic and inorganic groups chemically and increase cellulose-based substances (Marghaki et al., 2022; Hasan et al., 2021; Niu et al., 2021).

In recent years, green chemistry has been one of the essential aspects of chemists' experimental and industrial efforts (Ruijter and Orru, 2013; Wu et al., 2014; Cioc et al., 2014). Due to their atom efficiency and significant diversity, multi-component reactions (MCRs) have occupied an essential part of the green chemistry world (Jarrahi et al., 2021; Zhi et al., 2019; Sunderhaus and Martin, 2009; Biggs-Houck et al., 2010; Zareai et al., 2012). The multi-component reaction is a powerful synthetic strategy in modern chemistry in which three or more simple components as starting reagents are involved in a one-pot system to achieve new complex molecules at a less processing procedure in comparison to the step-by-step approach with usually few side-products (Váradi et al., 2016; Liu et al., 2019; Abdollahi-Basir et al., 2019; Jalili et al., 2021). Multi-component reactions have been widely used to synthesize critical heterocyclic compounds, which have many biological activities (Slobbe et al., 2012; Maleki et al., 2015; Wei et al., 2021). The pyrimidine family is one of the essential nitrogen-containing heterocycles due to their presence in many natural and biologically active products (Amin, 2009; Rashad et al., 2010; Singh et al., 2019). It is well known that the condensation of triazole and pyrimidine gives rise to the formation of bicyclic heterocycles known as triazolo pyrimidines, which exhibit a wide range of biological properties. Triazolo pyrimidines can be applied in various synthetic pharmacophores (Kolos et al., 2011; Gladkov et al., 2012; El-Gendy et al., 2008). Furthermore, they are valuable building blocks in the structure of many herbicidal drugs, such as penoxsulam, diclosulam, flumetsulam, azafenidin, and floransulan. Triazolopyrimidines are synthetic analogs of purines and nucleosides (Navarro et al., 1998; Magan et al., 2004; Magan et al., 2005). [1,2,4]Triazolo[1,5-a]pyrimidines, a subtype of purine bioisosteric analogs, were also reported to possess potential anti-tumor activities, especially those bearing functional groups at C-5, C-6, or C-7 positions (Traxler et al., 1996; Rusinov et al., 1986). Several synthetic strategies have been reported for the preparation of triazolo pyrimidine derivatives, most of which are based on the modification of the classical Biginelli reaction (Bhatt et al., 2016). Although some of these procedures are efficient, a number of them have limiting factors, including long reaction time, side reactions, rigid workup, high-temperature conditions, and non-recyclable reagents (Lauria et al., 2002).

In continuation of our efforts to synthesize a new heterogeneous nanocatalyst, in this study (keshavarz et al., 2022), we have reported the preparation and characterization of Fe_3O_4/MPC-[IL] as a supported Bronsted acidic ionic liquid catalyst. Moreover, the catalytic activity and reusability of the ionic liquid catalyst were examined for the synthesis of triazolo[4,3-a]pyrimidine derivatives.

2. Experimental

2.1. Methods and materials

All chemicals, as well as all solvents, were purchased from Merck, Aldrich-Sigma, and Fluka chemical companies and were used without further purification. Fourier-transform infrared spectrum was carried out in the region 400–4000 cm^{-1} by an FT-IR JASCO 6300D instrument. NMR spectra were taken with a Bruker 400 MHz Ultrashield spectrometer at 400 MHz (^{1}H) and 100 MHz (^{13}C) using DMSO d_6 as solvent. Melting points were determined in open capillaries using an electrothermal KSB1N-apparatus (Kruss, Germany). X-ray diffraction analysis was studied using a Rigaku Ultima IV, Japan diffractometer operated. Scanning electron microscopy was carried out by SEM: KYKY-EM3200 instrument operated at 26 kV. EDS was determined using the TESCAN vega model instrument. Thermo gravimetric (TGA) analyses were regulated using a Perkin Elmer STA 6000 instrument. The vibration sample-magnetometry (VSM) was monitored by the Kavir Magnet VSM. The surface area was investigated using the Brunauer-Emmett-Teller (BET) technique.

2.2. Synthesis of Fe_3O_4 NPs

$FeCl_3·6H_2O$ (2.3 g, 8.7 mmol) and $FeCl_2·4H_2O$ (0.86 g, 4.3 mmol) were mixed in distilled water (30 ml) under stirring and N_2 atmosphere at 80 °C for 30 min. Afterward, NaOH solution (10 ml, 25 %) was added dropwise to the mixture until the brown color solution turned out to the black and then was stirred for one h. The resulting product was collected using an external magnet and was washed with distilled water, and dried in an oven (Farahi et al., 2017).

2.3. Synthesis of 3-mercaptopropylcellulose (MPC)

The mixture of cellulose (1 g) and 3-mercaptopropyltrimethoxysilane (3 ml) in anhydrous toluene (40 ml) was stirred for 15 min at room temperature and then refluxed for 24 h. After this period, the mixture was filtered and repeatedly washed with anhydrous toluene and dried to obtain 3-mercaptopropylcellulose (MPC) (Carvalho et al., 2021).

2.4. Preparation of Fe_3O_4/MPC

In a round-bottomed flask (100 ml), the prepared Fe_3O_4 (1 g) was well dispersed in an aqueous solution (40 ml) containing NaOH (7 wt%) and urea (12 wt%) (ultrasonication for 10 min). Then 3-mercaptopropylcellulose (MPC) (1 g) was added to the flask, and the mixture was stirred for 1.5 h at −12 °C. After freezing for one h, the 3-mercaptopropylcellulose was dissolved fully. Ultimately, Fe_3O_4/MPC was collected with an external magnet, washed with deionized water, and dried in a vacuum oven for 24 h.

2.5. Preparation of acidic Bronsted ionic liquid [IL]

First, 1,4-butanesultone (12.2 g) was added to 1-vinyl imidazole (9.4 g) slowly at 0 °C. Then, the mixture was stirred at room temperature for about 24 h until it turned solid. The obtained solid was washed with diethyl ether and dried in a vacuum at 50 °C. Second, the prepared solid salt (2 g) was dissolved in H_2O (5 ml) in a 100 ml round bottom flask, and equal molar sulfuric acid was slowly dropped into the flask at 0 °C. Then the mixture was heated up to 60 °C gradually and then stirred for 12 h. Finally, the formed liquid was washed with diethyl ether and dried in a vacuum at 50 °C for six h.

2.6. Preparation of Fe₃O₄/MPC-[IL] (1)

For the synthesis of supported ionic liquid, the mixture of Fe_3O_4/MPC (1 g), [IL] (5 mmol), anhydrous toluene (100 ml), and azodiisobutyronitrile (AIBN) (5 mol %) were refluxed under N_2 atmosphere for 30 h. Finally, the product was washed with diethyl ether and dried under a vacuum.

2.7. General procedure for the synthesis of 5

A mixture of aldehyde (1 mmol), ethyl cyanoacetate or malononitrile (1 mmol), 3-amine-1H-1,2,4-triazole (1 mmol), and catalyst **1** (0.003 g) were stirred under solvent-free conditions at 100 °C. After completion of the process, monitored by TLC, hot ethanol (10 ml) was added, and the Fe_3O_4/MPC-[IL] was separated using an external magnet. Then, the pure product was obtained by recrystallization from EtOH. The recycled catalyst was washed with distilled water (10 ml) and ethanol (10 ml) and then dried at 100 °C. Finally, it was reused in subsequent runs.

2.8. Spectral data

Ethyl 5-amino-7-phenyl-7,8-dihydro-[1,2,4]triazolo[4,3-a]pyrimidine-6-carboxylate (**5a**). FT-IR (KBr) ($\bar{v}_{max}$, cm^{-1}): 3396, 3375, 3326, 2746, 1687, 1565, 1490, 1110. ¹H NMR (400 MHz, DMSO d_6): δ = 9.25 (s, 1H), 8.08 (d, 1H, J = 8 Hz), 7.66 (s, 2H), 7.57–7.64 (m, 5H) ppm, 5.37 (s, 1H), 3.93 (q, 2H, J = 8 Hz), 0.84 (t, 3H, J = 8 Hz). ¹³C NMR (100 MHz, DMSO d_6): δ = 162.28, 155.60, 133.90, 131.84, 131.28, 129.82, 116.09, 103.10, 24.96, 14.46.

Ethyl 5-amino-7-(4-chlorophenyl)-7,8-dihydro-[1,2,4]triazolo[4,3-a]pyrimidine-6-carboxylate (**5b**). FT-IR (KBr) ($\bar{v}_{max}$, cm^{-1}): 3412, 3253, 3115, 2872, 1692, 1532, 1485, 1203, ¹H NMR (400 MHz, DMSO d_6): δ = 9.25 (s, 1H), 8.08 (d, 1H, J = 8 Hz), 7.65 (s, 2H), 7.45–7.58 (m, 5H) ppm, 5.41 (s, 1H), 4.38 (q, 2H, J = 7 Hz), 0.92 (t, 3H, J = 7 Hz).¹³C NMR (100 MHz, DMSO d_6): δ = 163.83, 160.63, 154.82, 134.82, 130.96, 129.87, 129.04, 110.16, 61.09, 57.01, 14.02 ppm.

Ethyl 5-amino-7-(4-bromophenyl)-7,8-dihydro-[1,2,4]triazolo[4,3-a]pyrimidine-6-carboxylate (**5c**). FT-IR (KBr) ($\bar{v}_{max}$, cm^{-1}): 3427, 3389, 3098, 2923, 1677, 1587, 1488, 1178. ¹H NMR (400 MHz, DMSO d_6): δ = 9.16 (s, 1H), 8.39 (s, 2H), 7.41–7.43 (m, 5H) ppm, 7.08 (d, 1H, J = 3.6 Hz), 5.21 (s, 1H), 3.98 (q, 2H, J = 6.4 Hz), 1.33 (t, 3H, J = 6.6 Hz). ¹³C NMR (100 MHz, DMSO d_6): δ = 169.6, 156, 146, 141.99, 132.5, 129, 126.8, 62.1, 40.6, 27.5 ppm.

Ethyl 5-amino-7-(4-nitrophenyl)-7,8-dihydro-[1,2,4]triazolo[4,3-a]pyrimidine-6-carboxylate (**5d**). FT-IR (KBr) ($\bar{v}_{max}$, cm^{-1}): 3480, 3430, 3198, 2917, 1680, 1604, 1504, 1054. ¹H NMR (400 MHz, DMSO d_6) δ = 9.09 (s, 1H), 8.10 (d, 1H, J = 8 Hz), 7.83–7.91 (m, 4H), 5.99 (s, 1H), 4.43 (q, 2H, J = 7.2 Hz), 1.03 (t, 1H, J = 3.2 Hz) ppm. ¹³C NMR (100 MHz, DMSO d_6) δ = 163.62, 154.95, 149.60, 144.21, 134.01, 131.06, 130.42, 124.86, 124.46, 114.11, 63.57, 59.84, 14.00 ppm.

Ethyl 5-Amino-7-(3-nitrophenyl)-7,8-dihydro-[1,2,4]triazolo[4,3-a]pyrimidine-6-carboxylate (**5e**). FT-IR (KBr) ($\bar{v}$ $\bar{v}_{max}$, cm^{-1}): 3444, 3328, 3097, 2888, 1697, 1623, 1531, 1272. ¹H NMR (400 MHz, DMSO d_6): δ = 8.09 (d, 1H, J = 8 Hz), 7.80–7.83 (q, 4H), 6.41 (s, 1H), 5.69 (s, 1H), 4.03 (q, 2H, J = 8 Hz), 0.92 (t, 3H, J = 8 Hz) ppm. ¹³C NMR (100 MHz, DMSO d_6): δ = 163.63, 154.55, 150.36, 147.93, 134.84, 131.17, 130.83, 125.30, 123.78, 123.13, 113.63, 63.19, 59.06, 13.86 ppm.

Ethyl 5-amino-7-(2,4dichlorophenyl)-7,8-dihydro-[1,2,4]triazolo[4,3-a]pyrimidine-6-carboxylate (**5f**). FT-IR (KBr) ($\bar{v}_{max}$, cm^{-1}): 3489, 3421, 3085, 2878, 1699, 1586, 1474, 1106. ¹H NMR (400 MHz, DMSO d_6): δ = 11.67 (s, 1H), 8.11 (d, 1H, J = 8 Hz), 7.87 (s, 2H), 7.26–7.77 (t, 3H) ppm, 4.16 (s, 1H), 2.48 (q, 2H, J = 8 Hz), 1.25 (t, 3H, J = 7 Hz). ¹³C NMR (100 MHz, DMSO d_6): δ = 160.6, 153.6, 137.6, 130.2, 120.8, 127, 67.1, 40.4, 21.6 ppm.

Ethyl 5-amino-7-(4-methylphenyl)-7,8-dihydro-[1,2,4]-triazolo[4,3-a]pyrimidine-6-carbonitrile (**5 g**). FT-IR (KBr) ($\bar{v}_{max}$, cm^{-1}): 3347, 3262, 3185, 3118, 2921, 2192, 1660, 1633, 1531, 1482, 1363, 1286, 1214, 1157. ¹H NMR (400 MHz, DMSO d_6) δ = 8.75 (d, 1H, J = 1.6 Hz) ppm, 7.71 (s, 1H), 7.21 (s, 2H), 7.18 (s, 4H), 5.29 (d, 1H, J = 2.4 Hz), 2.28 (s, 3H). ¹³C NMR (100 MHz, DMSO d_6) δ = 153.92, 151.83, 146.93, 140.24, 137.26, 129.18, 126.00, 119.06, 56.06, 53.70, 20.64 ppm.

Ethyl 5-amino-7-(4-isopropylphenyl)-7,8-dihydro-[1,2,4]-triazolo[4,3-a]pyrimidine-6-carbonitrile (**5 h**). FT-IR (KBr) ($\bar{v}_{max}$, cm^{-1}): 3378, 3295, 3181, 3118, 2964, 2186, 1656, 1627, 1523, 1479, 1367, 1284, 1211, 1151. ¹H NMR (400 MHz, DMSO d_6) δ = 8.80 (d, 1H, J = 1.6 Hz) ppm, 7.76 (s, 1H), 7.24 (s, 4H), 7.31 (s, 2H), 5.33 (d, 1H, J = 2 Hz), 2.92 (s, 1H), 1.23 (d, 6H, J = 6.8 Hz). ¹³C NMR (100 MHz, DMSO d_6) δ = 153.91, 151.83, 148.21, 146.95, 140.71, 126.59, 125.99, 119.11, 55.97, 53.68, 33.11, 23.81 ppm.

3. Results and discussion

In this work, we report the preparation of Fe_3O_4/MPC-[IL] with high catalytic activity and its application in the synthesis of triazolo [4,3-a]-pyrimidines. The details of the preparation of magnetic nanoparticles supported by an acidic ionic liquid are presented in Scheme 1. Initially, the cellulose surface was functionalized with commercially available 3-mercaptopropyl trimethoxysilane (MPTMS) through siloxane linkages (MPC). Then, Fe_3O_4/MPC was fabricated through chemical modification of Fe_3O_4 nanoparticles with MPC in the presence of urea/NaOH. Afterward, the precursor ionic liquid was prepared using the reaction of 1-vinyl imidazole with 1,4-butane sultone, followed by treatment with sulfuric acid [IL]. Finally, Fe_3O_4/MPC-[IL] was synthesized by a radical grafting
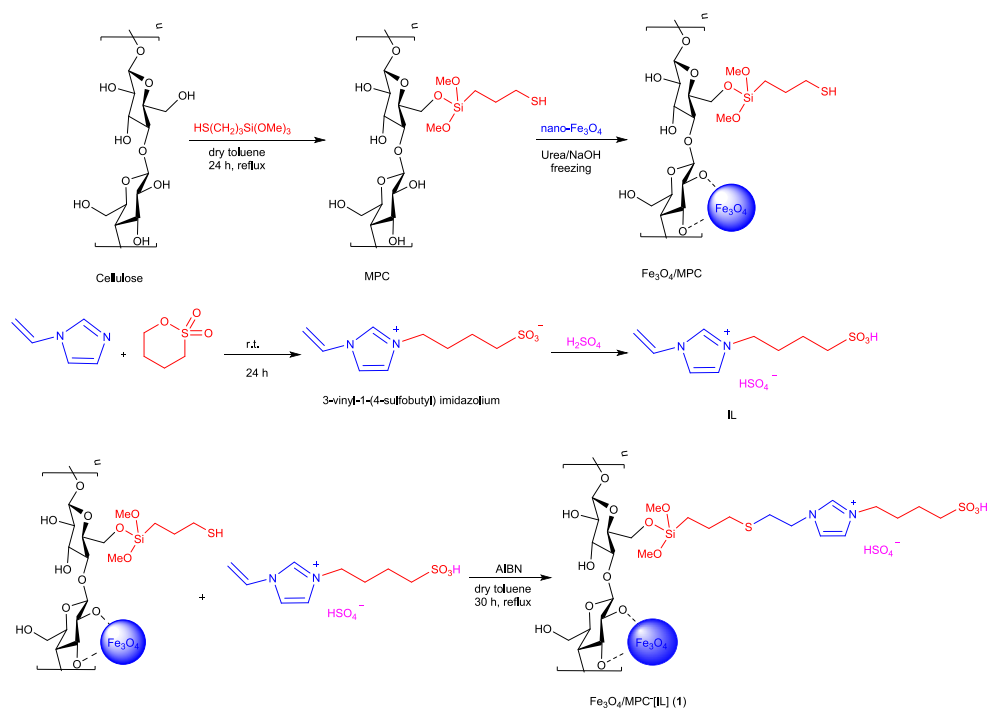
Scheme 1   Preparation of Fe₃O₄/MPC-[IL] (**1**).

copolymerization using the reaction of [IL] with Fe₃O₄/MPC. The prepared Fe₃O₄/MPC-[IL] was characterized using XRD, FT-IR, SEM map, EDS, SEM, VSM, TGA, and BET techniques.

Characterization by X-ray diffraction (XRD) was performed to investigate the structure of cellulose, Fe₃O₄, and Fe₃O₄/MPC-[IL] in a range of $2\theta = 10\text{-}80°$ (Fig. 1). The analysis of the XRD pattern of cellulose (Fig. 1a) shows three characterization peaks at $2\theta = 16.2°$, 18° and 24° assigned to the (1 1 0), (1 1 1) and (2 0 0) planes of crystalline cellulose (Jokar

et al., 2021; Zhang et al., 2019; Karami et al., 2018). In XRD pattern of Fe₃O₄, six characteristic peaks at $2\theta = 30.26°$, 35.7°, 43.5°, 53.59°, 57.5° and 63.26° were corresponding to the (2 2 0), (3 1 1), (4 0 0), (4 2 2), (5 1 1) and (4 4 0) crystal planes of a pure Fe₃O₄ with a spinal structure (Fig. 1b) (Dang et al., 2018; Ghanbari et al., 2018; Sadeghzadeh et al., 2014). XRD diffraction patterns were presented in Fig. 1c for the new catalyst Fe₃O₄/MPC-[IL]. As shown, on the path to the new catalyst synthesis, the diffraction pattern of cellulose was changed after functionalization
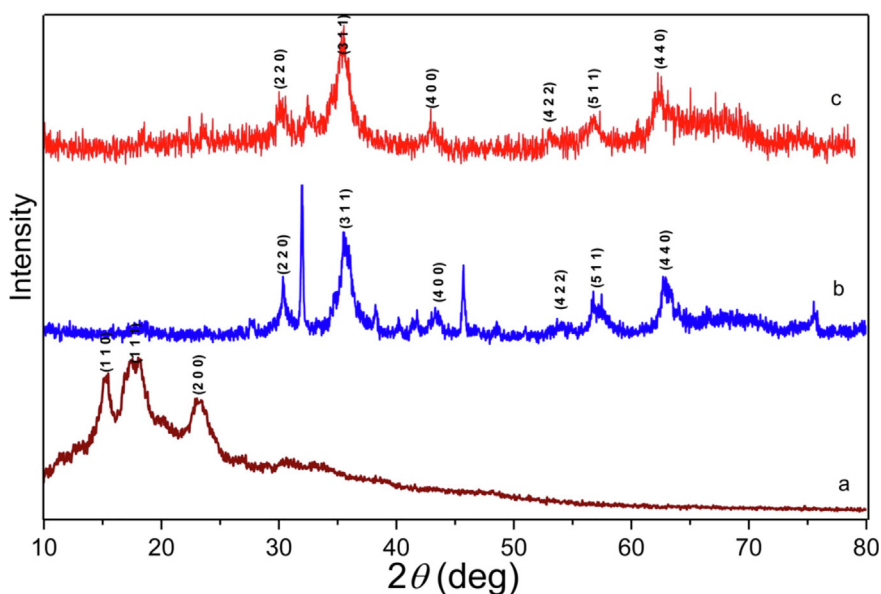

Fig. 1   XRD patterns of a) cellulose, b) Fe₃O₄, and c) Fe₃O₄/MPC-[IL].

with different layers and Fe_3O_4. In the pattern XRD, the Fe_3O_4/MPC-[IL] nanocatalyst show that severities of peaks declined; however, comparing Fig. 1c with Fig. 1a and 1b confirms the stabilization of the Fe_3O_4 nanoparticles with IL on cellulose and Fe_3O_4/MPC-[IL] nanocatalyst was successfully synthesized.

The FT-IR analyses of cellulose, MPC, Fe_3O_4, Fe_3O_4/MPC, [IL], and Fe_3O_4/MPC-[IL] were performed to prove their synthesis at each step. In Fig. 2a, the broad peak at 3350 cm^{-1} is attributed to the stretching vibration of the hydroxy groups of cellulose. The band at 1462 cm^{-1} is related to the bending vibrations of H—C—H and O—C—H (Fig. 2a) (Liu et al., 2021; Heidari and Aliramezani, 2021). The peaks of symmetric and asymmetric vibrations of the Si-O bond were seen at 973 and 1140 cm^{-1}. The typical peak of the thiol group (S—H) was observed at 2550 cm^{-1} (Fig. 2b) (Jankauskaite et al., 2020; Shang et al., 2018; Loof et al., 2016). The spectra of the blank Fe_3O_4 show that the peak at 580 cm^{-1} could be due to the Fe–O vibration (Fig. 2c) (Maleki et al., 2017; Zhang et al., 2019). The presence of the characteristic absorption peak of Fe-O in all compared spectra is a confirmation of how nanoparticles of Fe_3O_4 have remained during the process (Fig. 2d and Fig. 2f). The IR curve of IL shows typical bands at 1563 cm^{-1} can be assigned to the imidazolium ring (C=C, C=N). The peaks at around 3143 cm^{-1} correspond to the C—H stretching vibration of imidazole moiety (sp^2) (Zhang et al., 2012a, 2012b; Zhang et al., 2018). The bands around 1039 cm^{-1} and 1165 cm^{-1} were associated with the signals of C—S and S=O bonds, indicating the existence of the -SO_3H group (Fig. 2e) (Qiao et al., 2006). However, the peak of S—H at 2565 cm^{-1} and end-group C=C totally at 1647 cm^{-1} disappeared, while the peak of the imidazole ring at 1563 cm^{-1} remained after a radical chain transfer reaction between modified cellulose and ionic liquid occurred (Fig. 2f), which convinced us that the [($CH_2)_3SO_3$HVIm] HSO_4 ionic liquid was successfully grafted on functionalized cellulose via the route shown in Scheme 1.

The element mapping analysis of the Fe_3O_4/MPC-[IL] nanocatalyst was shown in Fig. 3. As can be seen, all elements (C, Si, Fe, O, S, and N) are uniformly distributed on the surface of the catalyst, which indicates the successful immobilization of expected elements on cellulose.

The EDX analysis confirmed the presence of the desired elements in the Fe_3O_4/MPC-[IL] nanocatalyst. As shown, the peaks of C, Fe, Si, O, N and S are observed in the EDX spectrum, and these elements confirm that the magnetite NPs and ionic liquid are successfully immobilized onto functionalized cellulose surface and the desired catalyst has been synthesized (Fig. 4).

The morphology and size of the Fe_3O_4 and Fe_3O_4/MPC-[IL] were investigated using scanning electron microscopy (SEM) (Fig. 5). These images confirm the formation of the desired nanoparticles with spherical morphology. The average nanoparticles diameter of Fe_3O_4/MPC-[IL] is around 56–73 nm.

The transmission electronic microscopy (TEM) images of Fe_3O_4/MPC-[IL] nanocatalyst are shown in Fig. 6. These images indicate magnetite NPs black cores surrounded by a gray shell of modified cellulose. Furthermore, the TEM images showed that nanoparticles were composed of relatively small and almost spherical particles.

The magnetic properties of Fe_3O_4 and Fe_3O_4/MPC-[IL] nanoparticles were investigated using the VSM technique. As shown in Fig. 7, VSM measurements for Fe_3O_4 nanoparticles show that the saturation magnetization is 53.03 emu/g, while the saturation magnetization of Fe_3O_4/MPC-[IL] is decreased to 15.2 emu/g. The free MNPs show a higher magnetic valence in comparison with functionalized Fe_3O_4, which this result is due to the coated cellulose and the ionic liquid that joined to support.

In the next step, the thermal stability of the catalyst was studied using TGA (Fig. 8). These were performed from 30 to 900 °C, showing the TGA curve of Fe_3O_4/MPC-[IL], which this analysis confirms the stability and presence of fixed groups on nanostructures. As can be seen in the TGA curve of the prepared Fe_3O_4/MPC-[IL], it has an initial weight loss of about 3.5 % up to 180 °C, which was attributed to desorption of physically adsorbed solvents, surface hydroxyl groups, and
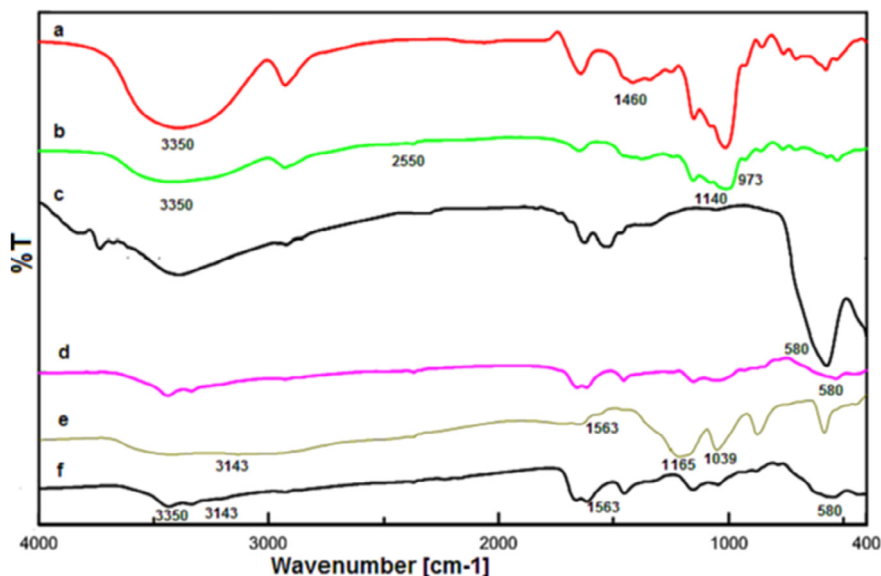

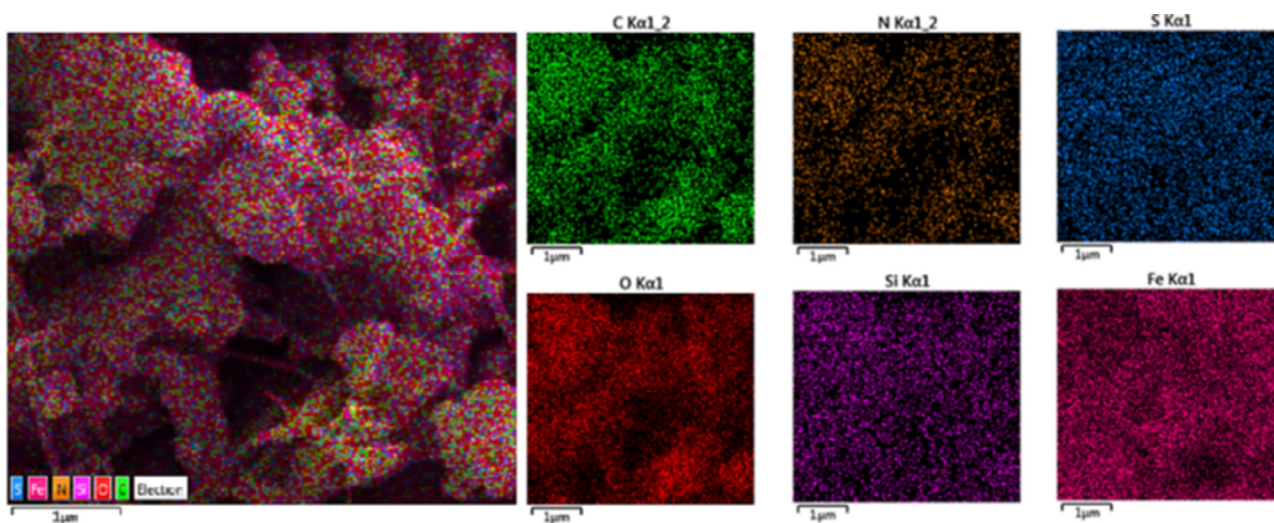**Fig. 2** FT-IR spectra of a) cellulose, b) MPC, c) Fe_3O_4, d) Fe_3O_4/MPC, e) [IL] and f) Fe_3O_4/MPC-[IL].

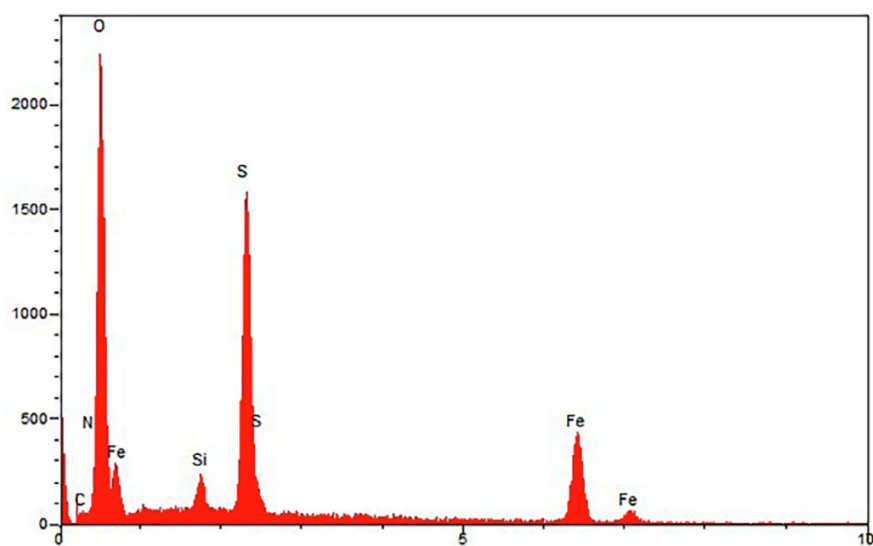**Fig. 3**   Elemental mapping analysis of Fe$_3$O$_4$/MPC-[IL] nanocatalyst.

Fig. 4   Energy dispersive X-ray spectroscopy (EDS) result for Fe$_3$O$_4$/MPC-[IL] nanocatalyst.
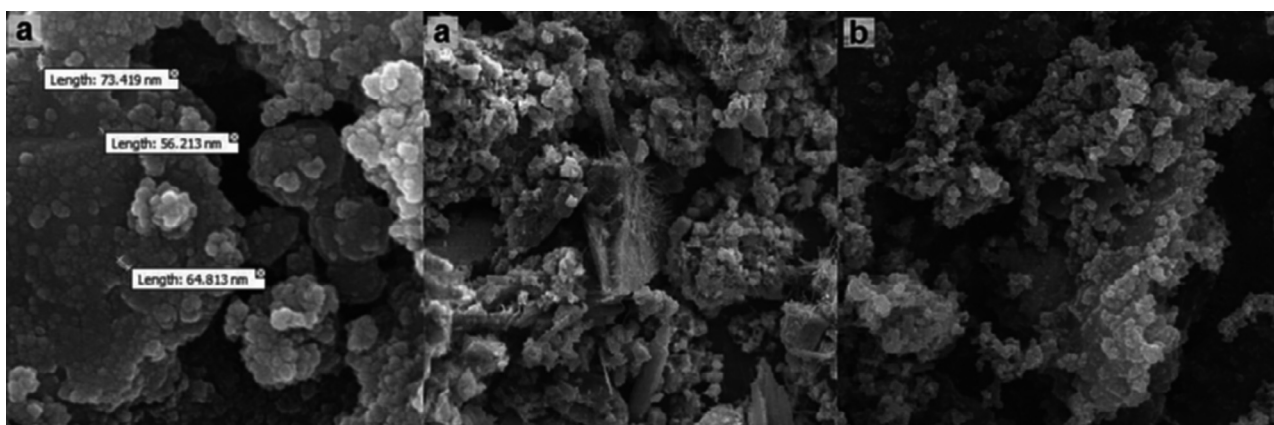
Fig. 5   FE-SEM images of a) Fe$_3$O$_4$/MPC-[IL] and b) Fe$_3$O$_4$.
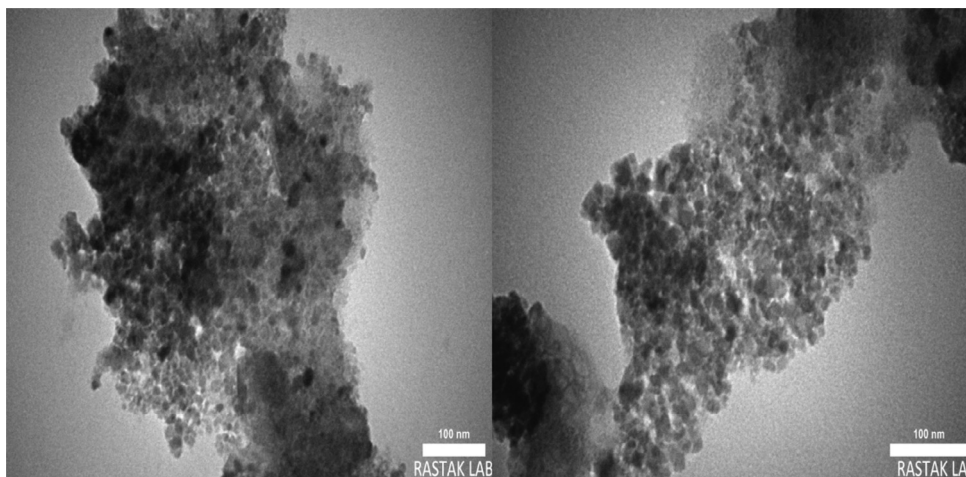
Fig. 6 TEM images of the Fe_3O_4/MPC-[IL] nanocatalyst.
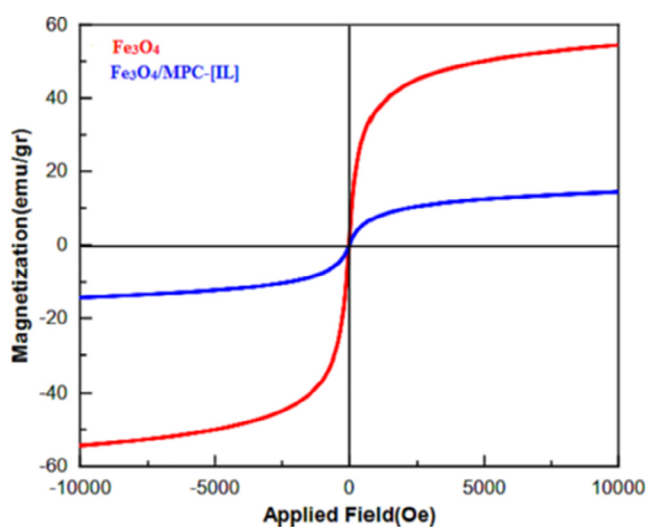
Fig. 7 VSM analysis of Fe_3O_4 and Fe_3O_4/MPC-[IL].
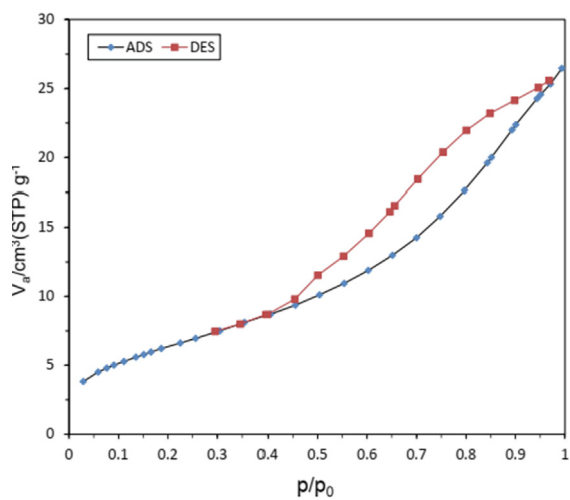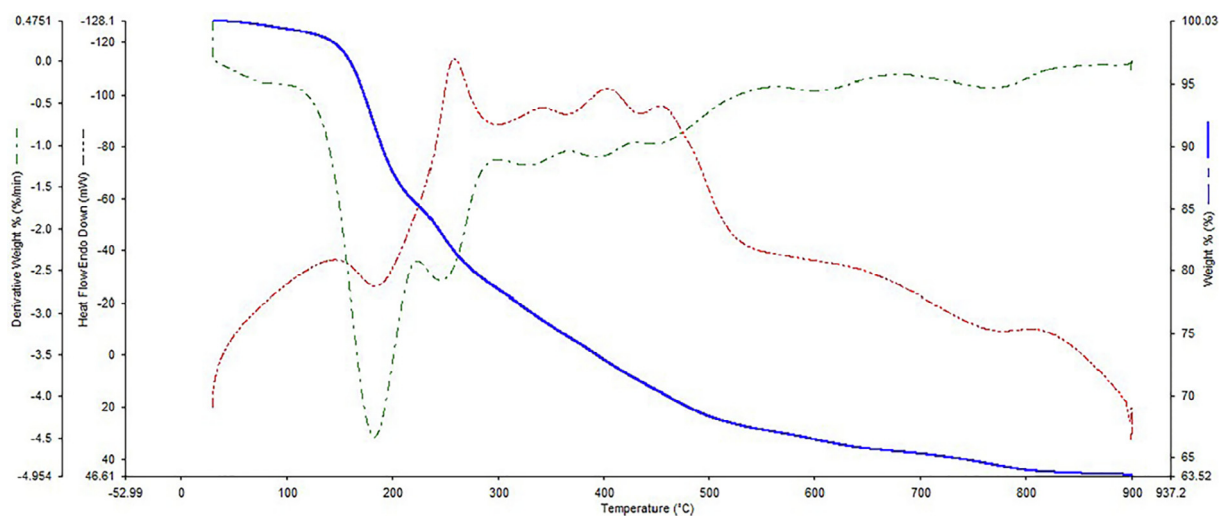

Fig. 9 BET of Fe_3O_4/MPC-[IL] catalyst.

Fig. 8 TGA curve of Fe_3O_4/MPC-[IL] **1**.

structural water. The second and significant weight loss occurs between 180 and 550 °C, showing a weight loss of 30 %, which may be related to the decomposition of organic groups, amine groups, and removal of the sulfuric acid group on the surface of the nanocatalyst. The last weight loss between 550 and 900 °C, with an observed weight loss of 4 %, is related to the immobilized organic groups grafting to the cellulose surface and confirms the stability of the synthesized nanocatalyst.

In the following, the surface area of the solid acid catalyst Fe_3O_4/MPC-[IL] was investigated using the N_2 adsorption–desorption curve (Fig. 9). According to the IUPAC classification, the Fe_3O_4/MPC-[IL] nanocomposite reveals a type IV isotherm with an H1 hysteresis loop. Based on this analysis, the area of the surface 23.92 m^2g^{-1}, the total volume of the pores 5.49 cm^3g^{-1} and the mean pores diameter 6.79 nm were obtained.

After successful preparation and characterization, Fe_3O_4/MPC-[IL] was applied as an effective nanocatalyst in the synthesis of triazolo[4,3-a]-pyrimidines derivatives **5** (Scheme 2).

To optimize the reaction conditions, the effect of catalyst, solvent and temperature was investigated in the reaction of benzaldehyde (1 mmol), ethyl cyanoacetate (1 mmol), and 3-amine-1H-1,2,4-triazole (1 mmol) as the model reaction. In the first step, the effect of catalyst loading in the reaction progress was studied under solvent-free conditions, and the

desired product was not produced without a catalyst. The best result was conducted in the presence of 0.003 g of catalyst **1**. Furthermore, the model reaction was performed by 0.003 g of Fe_3O_4/MPC-[IL] in some solvents such as EtOH, EtOH:H_2O, MeOH, H_2O, DMF, DMSO, and toluene. As can be seen, considerable acceleration is observed chiefly in reactions performed under solvent-free conditions. Next, the effect of the temperature was studied. We performed the reaction at different temperatures, and the reaction at 100 °C gave the best result. The results of this study are summarized in Table 1. According to these results, using Fe_3O_4/MPC-[IL] (0.003 g) as a catalyst under solvent-free conditions at 100 °C would be the best choice.

To investigate the generality of this protocol, different aryl aldehydes containing both electron-donating and electron-withdrawing groups were employed in the reaction. The reaction proceeded smoothly to afford the desired products **5** in good to excellent yields. Furthermore, under similar conditions, aryl aldehydes and 3-amine-1H-1,2,4-triazole were reacted with malononitrile in the presence of catalyst **1**. The obtained results are summarized in Table 2.

According to the reported mechanisms in the literature (Ablajan et al., 2012), we proposed a plausible mechanism for the synthesis of [1,2,4]-triazolo[4,3-a]-pyrimidines (**5**) (Scheme 3). Initially, aldehyde (**2**) is activated by the acidic sur-

R: CN, CO_2Et
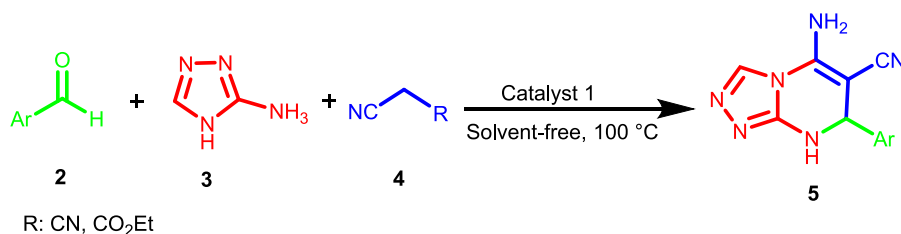
Scheme 2   Synthesis of triazolo [4,3-a]-pyrimidines derivatives **5** in the presence of nanocatalyst **1**.

Table 1   Optimization of the reaction conditions.[a]

Entry	Catalyst **1** (g)	Solvent	Temp. (°C)	Yield (%)[b]
1	–	–	25	–
2	–	–	80	5
3	–	–	90	8
4	–	–	100	9
5	0.001	–	100	60
6	0.003	–	100	90
7	0.005	–	100	85
8	0.007	–	100	85
9	0.003	Ethanol	reflux	25
10	0.003	EtOH:H_2O	reflux	34
11	0.003	Methanol	reflux	38
12	0.003	H_2O	100	43
13	0.003	DMF	100	20
14	0.003	DMSO	100	35
15	0.003	Toluene	100	23
16	0.003	–	80	75
17	0.003	–	110	90
18	0.003	–	120	85

[a] Reaction conditions: benzaldehyde (1 mmol), ethyl cyanoacetate (1 mmol), 3-amine-1H-1,2,4-triazole (1 mmol), time: 20 min. [b] Isolated yields.

Table 2 Synthesis of compounds **5** in the presence of Fe_3O_4/MPC-[IL].[a]

Entry	Aldehyde	Product **5**	Yield (%)[b]	M. p. (°C)	References
5a	C_6H_4CHO		96	189-191[c]	–
5b	4-Cl C_6H_4CHO		92	190-191[c]	–
5c	4-Br C_6H_4CHO		93	184-184[c]	–
5d	4-NO_2 C_6H_4CHO		92	194-196[c]	–
5e	3-NO_2 C_6H_4CHO		95	190-192[c]	–
5f	2,4-Cl_2 C_6H_3CHO		96	243-245[c]	–
5 g	4-CH_3 C_6H_4CHO		92	243–245	Ablajan et al., (2012)
5 h	4-i-Pr C_6H_4CHO		93	218-220[c]	–
5i	4-NO_2 C_6H_4CHO		92	245–247	Ablajan et al., (2012)
5j	2-Cl C_6H_4CHO		94	263–266	Ablajan et al., (2012)

(*continued on next page*)

Table 2 (*continued*)

Entry	Aldehyde	Product **5**	Yield (%)[b]	M. p. (°C)	References
5 k	4-Br C_6H_4CHO		95	264–266	Ablajan et al., (2012)
5 l	4-Cl C_6H_4CHO		97	257–258	Ablajan et al., (2012)
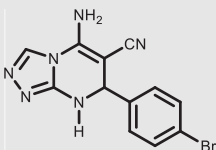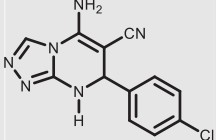
[a] Reaction conditions: aryl aldehyde (1 mmol), ethyl cyanoacetate or malononitrile (1 mmol), 3-amine-1H-1,2,4-triazole (1 mmol), catalyst **1** (0.003 g), solvent-free, 100 °C. [b] Isolated yield. [c] Novel compound.
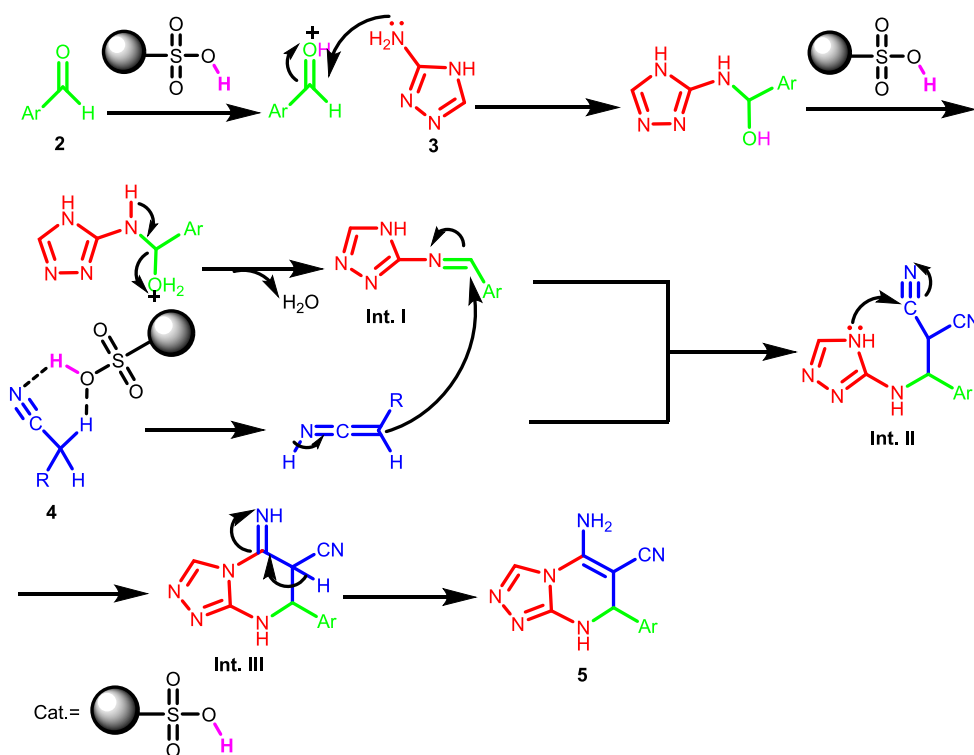
Scheme 3   Proposed mechanism for synthesizing **5** in the presence of Fe_3O_4/MPC-[IL] as a catalyst.

face sites of the catalyst. Next, the catalyst-activated aldehyde is attacked by 3-amine-1H-1,2,4-triazole (**3**), followed by the elimination of water to form intermediate **I**. Then, compound **4** performs a Michael-type addition to intermediate **I** to give intermediate **II**. The desired product **5** was obtained after the intramolecular cyclization and tautomerization intermediate **III** (Scheme 3).

In the subsequent study, a leaching experiment was performed in the model reaction. When the reaction progress reached 50 %, hot EtOH (5 ml) was added, and the catalyst was magnetically separated and removed. After removing the solvent, the reaction of residue was screened under optimal conditions. Interestingly, no remarkable product was obtained in the reaction progress, indicating that the catalyst operates heterogeneously. The most important advantage of the applied catalyst is recoverability and reusability. It is important to note
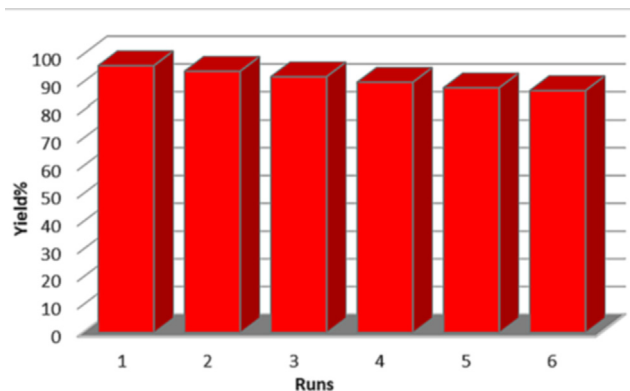
Fig. 10   Reusability of the heterogeneous nanocatalyst **1** for the synthesis of **5a**.
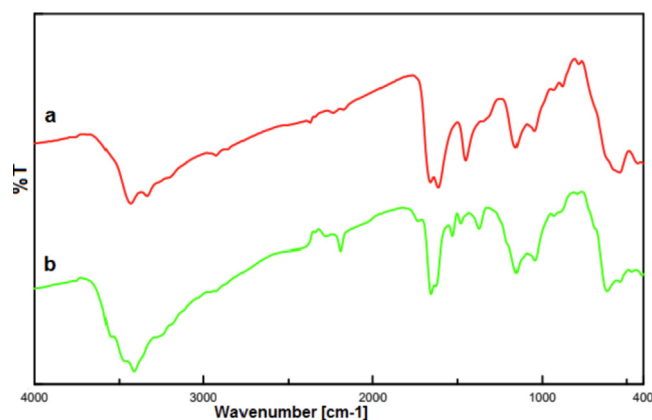
Fig. 11 FT-IR spectrum of a) Fe_3O_4/MPC-[IL] and b) recycled Fe_3O_4/MPC-[IL].
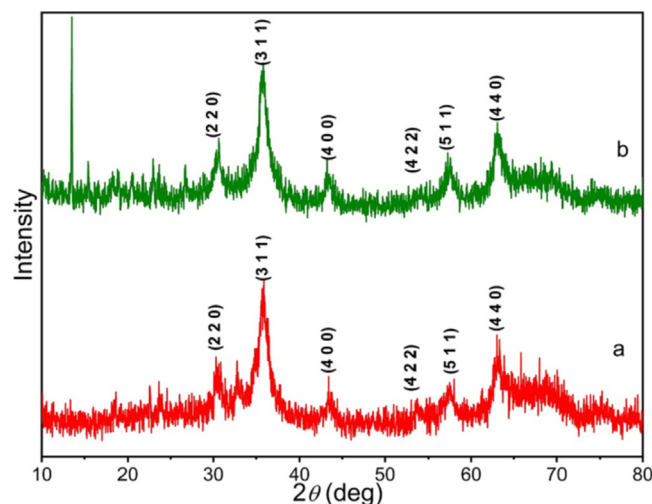

Fig. 12 The XRD pattern of a) Fe_3O_4/MPC[IL] and b) recycled Fe_3O_4/MPC[IL].

that the magnetic property of this catalyst facilitates its efficient recovery from the final products. Furthermore, we examined the recyclability of Fe_3O_4/MPC-[IL] in the model reaction. After completion of the reaction, EtOH (5 ml) was added to the mixture, and the catalyst was filtered and washed with distilled water three times by ethanol, followed by drying at 100 °C. Applying the recovered catalyst for six successive runs in the model reaction generated the product, having a low reduction in yield (Fig. 10). These experiments indicate the high stability and durability of this nanocatalyst under the applied conditions.

FT-IR spectrums of the Fe_3O_4/MPC-[IL] and recycled catalyst are shown in Fig. 11. This spectrum confirms good stability of the structure of Fe_3O_4/MPC-[IL] after recycling. The structural properties of the Fe_3O_4/MPC-[IL] and recycled catalyst were analyzed by XRD. This spectrum indicates structural stability; as shown in Fig. 12, the position and relative intensities of all peaks confirm this well.

Next, we compared the efficiency of Fe_3O_4/MPC[IL] nanocatalyst with previous catalysts utilized recently in the synthesis of triazolo[4,3-*a*]pyrimidine derivatives (Table 3). As shown, Fe_3O_4/MPC[IL] is a catalyst with high durability, stability, recycling times, reaction time, and increased product yield better than the other catalysts.

4. Conclusions

Herein, given one of the bases of green chemistry, we introduced Fe_3O_4/MPC[IL] as a novel Fe3O4-cellulose-supported ionic liquid. Structural characterization was performed using XRD, FT-IR, EDX, SEM, VSM, TGA, and BET. Finally, this new nanocatalyst as an efficient heterogeneous catalyst with the ability to be recyclable and reusable, biocompatible, easy separation, wide substrate tolerance, high atom economy, mild reaction conditions, good to excellent yields, and short reaction times for the synthesis of triazolo[4,3-*a*]pyrimidine derivatives are the major important features of this new catalytic system. Also, the catalyst can be quickly recovered using a simple external magnet and reused several times without significantly losing its catalytic activity. The results of this study give us hope that it will be used in the future to synthesize other reactions and organic compounds.

Table 3 The comparison study between the efficiency of the Fe_3O_4/MPC[IL] heterogeneous catalyst with that of other catalysts in the synthesis of triazolo[4,3-*a*]pyrimidine.

Catalyst	Conditions	Time (min)	Yield (%)	Recovery times	References
Bi_2O_3/FAp	Cat. (30 mg), EtOH, r. t.	25–35	92–96	5	Kerru et al., 2020
TMDP	Cat. (10.5 mg), Solvent-free, 50 °C	35–70	71–93	–	Zaharani et al., 2020
TMDPS	Cat. (1 ml), Neat, r. t.	105–150	73–94	–	Zaharani et al., 2020
NaOH	Cat. (20 mol %), Ultrasonic, 25–35 °C EtOH	60	35–88	–	Ablajan et al., 2012
mPMF	Cat. (20 mg), 600 rpm, Solvent-free, r. t.	90	76–94	5	Khaligh and Mihankhah, 2022
3-vinyl-1-(4-sulfobutyl) imidazolium	Cat. (0.01 g), Solvent-free, 100 °C	20	–	–	This work
IL	Cat. (1 ml), Solvent-free, 100 °C	20	–	–	This work
Fe_3O_4/MPC[IL]	Cat.(0.003 g), Solvent-free, 100 °C	15–20	90–97	6	This work

Declaration of Competing Interest

The authors declare that they have no known competing financial interests or personal relationships that could have appeared to influence the work reported in this paper.

Appendix A. Supplementary material

Supplementary data to this article can be found online at https://doi.org/10.1016/j.arabjc.2022.104311.

References

Abdelhameed, R.M., El-Shahat, M., Emam, H.E., 2020. Employable metal (Ag & Pd)@MIL-125-NH$_2$@cellulose acetate film for visible-light driven photocatalysis for reduction of nitro-aromatics. Carbohydr. Polym. 247, 116695–116721. https://doi.org/10.1016/j.carbpol.2020.116695.

Abdollahi-Basir, M.H., Shirini, F., Tajik, H., Ghasemzadeh, M.A., 2019. MIL-53(Fe): Introduction of a new catalyst for the synthesis of Pyrimido[4,5-d]pyrimidine derivatives under solvent-free conditions. J. Mol. Struct. 1197, 318–325. https://doi.org/10.1016/j.molstruc.2019.07.065.

Ablajan, K., Kamil, W., Tuoheti, A., Wan-Fu, S., 2012. An efficient three component one-pot synthesis of 5-amino-7-aryl-7,8-dihydro-[1,2,4] triazolo[4,3-a]-pyrimidine-6-carbonitriles. Molecules 17, 1860–1869. https://doi.org/10.3390/molecules17021860.

Amin, K.M., Hanna, M.M., Abo-Youssef, H.E., George, R.F., 2009. Synthesis, analgesic and anti-inflammatory activities evaluation of some bi-, tri- and tetracyclic condensed pyrimidines. Eur. J. Med. Chem. 44, 4572–4584. https://doi.org/10.1016/j.ejmech.2009.06.028.

Atghia, S.V., Sarvi-Beigbaghlou, S., 2013. Nanocrystalline titania-based sulfonic acid (TiO$_2$-Pr SO$_3$H) as a new, highly efficient and recyclable solid acid catalyst for the N-Boc protection of amines at room temperature. J. Appl. Organomet. Chem. 745, 42–49. https://doi.org/10.1016/j.jorganchem.2013.07.03.

Azizi, N., Shirdel, F., 2016. Task specific dicationic acidic ionic liquids catalyzed efficient and rapid synthesis of benzoxanthenones derivatives. J. Mol. Liq. 222, 783–787. https://doi.org/10.1016/j.molliq.2016.07.128.

Bhatt, J.D., Chudasama, C.J., Patel, K.D., 2016. Microwave assisted synthesis of pyrimidines in ionic liquid and their potency as non-classical malarial antifolates. Arch. Pharm. 349, 791–800. https://doi.org/10.1002/ardp.201600148.

Biggs-Houck, J.E., Younai, A., Shaw, J.T., 2010. Recent advances in multicomponent reactions for diversity-oriented synthesis. Curr. Opin. Chem. Bio. 14, 371–382. https://doi.org/10.1016/j.cbpa.2010.03.003.

Carvalho, A.L.C.B., Ludovici, F., Goldmann, D., Silva, A.C., Liimatainen, H., 2021. Silylated thiol-containing cellulose nanofibers as a bio-based flocculation agent for ultrafine mineral particles of chalcopyrite and pyrite. J. Sustain. Metall. 7, 1506–1522. https://doi.org/10.1007/s40831-021-00439-y.

Cioc, R., Uijter, R.E., Orru, R.V., 2014. Multicomponent reactions: advanced tools for sustainable organic synthesis. Green Chem. 16, 2958–2975. https://doi.org/10.1039/C4GC00013G.

Cole, A.C., Jensen, J.L., Ntai, I., Tran, K.L.T., Weaver, K.J., Forbes, D.C., Davis, J.H., 2002. Novel Brønsted acidic ionic liquids and their use as dual solvent-catalysts. J. Am. Chem. Soc. 124, 5962–5963. https://doi.org/10.1021/ja026290w.

Dang, B., Chen, Y., Wang, H., Chen, B., Jin, C., Sun, Q., 2018. Preparation of high mechanical performance nano-Fe$_3$O$_4$/wood fiber binderless composite boards for electromagnetic absorption via a facile and green method. Nanomater. 8, 52–68. https://doi.org/10.3390/nano8010052.

Elavarasan, P., Rengadurai, S., Upadhyayula, S., 2020. Kinetics of phenol alkylation with tert-butyl alcohol using supported ionic liquid catalyst. Adv. Chem. Eng. 4, 100045–100053. https://doi.org/10.1016/j.ceja.2020.100045.

El-Gendy, M.M.A., Shaaban, M., Shaaban, K.A., El-Bondkly, A.M., Laatsch, H., 2008. Essramycin: A first triazolopyrimidine antibiotic isolated from nature. J. Antibiot. 61, 149–157. https://doi.org/10.1038/ja.2008.124.

Farahi, M., Karami, B., Keshavarz, R., Khosravian, F., 2017. Nano-Fe$_3$O$_4$@SiO$_2$-supported boron sulfonic acid as a novel magnetically heterogeneous catalyst for the synthesis of pyrano coumarins. RSC Adv. 7, 46644–46650. https://doi.org/10.1039/c7ra08253c.

Ghanbari, M., Moradi, S., Setoodehkhah, M., 2018. Fe$_3$O$_4$@SiO$_2$@-ADMPT/H$_6$P$_2$W$_{18}$O$_{62}$: A novel Wells-Dawson heteropolyacid-based magnetic inorganic–organic nanohybrid material as potent lewis acid catalyst for the efficient synthesis of 1,4-dihydopyridines. Green Chem. Lett. Rev. 11, 111–124. https://doi.org/10.1080/17518253.2018.1445781.

Gladkov, E.S., Gura, K.A., Sirko, S.M., Desenko, S.M., Groth, U., Chebanov, V.A., 2012. Features of the behavior of 4-amino-5-carboxamido-1,2,3-triazole in multicomponent heterocyclizations with carbonyl compounds. Beilstein J. Org. Chem. 8, 2100–2105. https://doi.org/10.3762/bjoc.8.236.

Greer, A.J., Jacquemin, J., Hardacre, C., 2020. Industrial applications of ionic liquids. Molecules 25, 5207–5238. https://doi.org/10.3390/molecules25215207.

Hamdy, M.S., Eissa, M.A., Keshk, S.A., 2017. New catalyst with multiple active sites for selective hydrogenolysis of cellulose to ethylene glycol. Green Chem. 19, 5144–5151. https://doi.org/10.1039/C7GC02122D.

Han, S., Yang, J., Huang, H., 2022. Novel self-solidifying double-site acidic ionic liquid as efficient and reusable catalyst for green biodiesel synthesis. Fuel 315, 122815–122824. https://doi.org/10.1016/j.fuel.2021.122815.

Hasan, M.J., Petrie, F.A., Johnson, A.E., Peltan, J., Gannon, M., Busch, R.T., Vasquez, E.S., Urena-Benavides, E.E., 2021. Magnetically induced demulsification of water and castor oil dispersions stabilized by Fe$_3$O$_4$-coated cellulose nanocrystals. Cellulose 28, 4807–4823. https://doi.org/10.1007/s10570-021-03813-x.

Heidari, H., Aliramezani, F., 2021. Reductant-free and in-situ green synthesis of Ag nanoparticles on Fe$_3$O$_4$@nanocellulose and their catalytic activity for the reduction of dyes. Chemistry Select 6, 1223–1229. https://doi.org/10.1002/slct.202004579.

Jalili, Z., Tayebee, R., Zonoz, F.M., 2021. Eco-friendly synthesis of chromeno[4,3-b]chromenes with a new photosensitized WO$_3$/ZnO@NH$_2$-EY nanocatalyst. RSC Adv. 11, 18026–18039. https://doi.org/10.1039/d0ra09737c.

Jamshidi, A., Maleki, B., Zonoz, F.M., Tayebee, R., 2018. HPA-dendrimer functionalized magnetic nanoparticles (Fe$_3$O$_4$@D-NH$_2$-HPA) as a novel inorganic-organic hybrid and recyclable catalyst for the one-pot synthesis of highly substituted pyran derivatives. Mater. Chem. Phys. 209, 46–59. https://doi.org/10.1016/j.matchemphys.2018.01.070.

Jankauskaite, V., Balciunaitien, A., Alexandrova, R., Buskuvien, N., Zukiene, K., 2020. Effect of cellulose microfiber silylation procedures on the properties and antibacterial activity of polydimethylsiloxane. Coatings 10, 567–590. https://doi.org/10.3390/coatings10060567.

Jarrahi, M., Tayebee, R., Maleki, B., Salimi, A., 2021. One-pot multicomponent green LED photoinduced synthesis of chromeno [4,3-b]chromenes catalyzed by a new nanophotocatalyst histaminium tetrachlorozincate. RSC Adv. 11, 19723–19736. https://doi.org/10.1039/d1ra00189b.

Jokar, M., Naeimi, H., Nabi-Bidhendi, G., 2021. Preparation and characterization of cellulose sulfate/Pd nanocatalsysts with remarkable efficiency for Suzuki-Miyaura reaction. J. Appl. Organomet. Chem. 35, 6266–6275. https://doi.org/10.1002/aoc.6266.

Kamel, S., Khattab, T.A., 2021. Recent advances in cellulose supported metal nanoparticles as green and sustainable catalysis for organic synthesis. Cellulose 28, 4545–4574. https://doi.org/10.1007/s10570-021-03839-1.

Karami, S., Zeynizadeh, B., Shokri, Z., 2018. Cellulose supported bimetallic Fe-Cu nanoparticles: a magnetically recoverable nanocatalyst for quick reduction of nitroarenes to amines in water. Cellulose 25, 3295–3305. https://doi.org/10.1007/s10570-018-1809-0.

Kerru, N., Gummidi, L., Maddila, S.N., Bhaskaruni, S.V.H.S., Jonnalagadda, S.B., 2020. Bi2O3/FAp, a sustainable catalyst for synthesis of dihydro-[1,2,4] triazolo [1,5-a] pyrimidine derivatives through green strategy. Appl. Organomet. Chem. 34, 5590–5599. https://doi.org/10.1002/aoc.5590.

Keshavarz, R., Farahi, M., Karami, B., Gheibipour, P., Zarnegaryan, A., 2022. TiO2-coated graphene oxide-molybdate complex as a new separable nanocatalyst for the synthesis of pyrrole derivatives by Paal-Knorr reaction. Arab. J. Chem. 15,. https://doi.org/10.1016/j.arabjc.2022.103736 103736.

Khaligh, N.G., Mihankhah, T., 2022. Green and solid-phase synthesis of new dihydro-[1, 2, 4] triazolo [1, 5-a] pyrimidine scaffolds by using poly-melamine-formaldehyde as a nitrogen-rich porous organocatalyst. Polycycl. Aromat. Compd. 42, 942–950. https://doi.org/10.1080/10406638.2020.1756357.

Khoshnevis, M., Davoodnia, A., Zare-Bidaki, A., Tavakoli-Hoseini, N., 2013. Alumina supported acidic ionic liquid: Preparation, characterization, and its application as catalyst in the synthesis of 1,8-dioxo-octahydroxanthenes. Synth. React. Inorg. Met. 43, 1154–1161. https://doi.org/10.1080/15533174.2012.756897.

Kolos, N.N.S., Kovalenko, L.U., Borovskoy, V.A., 2011. Reactions of 3-aroylacrylates with α-aminoazoles. Chem. Heterocycl. Comp. 47, 983–988. https://doi.org/10.1007/s10593-011-0864-3.

Lauria, A., Diana, P., Barraja, P., Montalbano, A., Cirrinicione, G., Dattolo, G., Almerico, A.M., 2002. New tricyclic systems of biological interest. Annelated 1,2,3-triazolo[1,5-a]pyrimidines through domino reaction of 3-azidopyrroles and methylene active nitriles. Tetrahedron 58, 9723–9727. https://doi.org/10.1016/S0040-4020(02)01245-0.

Li, R., Jiang, Y., Zhao, J., Ramella, D., Peng, Y., Luan, Y., 2017. Development of a Brønsted acid Al–MIL-53 metal–organic framework catalyst and its application in [4 + 2] cycloadditions. RSC. Adv. 7, 34591–34597. https://doi.org/10.1039/C7RA06201J.

Li, B.L., Zhang, M., Hu, H.C., Du, X., Zhang, Z.H., 2014b. Nano-CoFe2O4 supported molybdenum as an efficient and magnetically recoverable catalyst for a one-pot, four-component synthesis of functionalized pyrroles. New J. Chem. 38, 2435–2442. https://doi.org/10.1039/C3NJ01368E.

Li, Z.M., Zhou, Y., Tao, D.J., Huang, W., Chen, X.S., Yang, Z., 2014a. MOR zeolite supported Brønsted acidic ionic liquid: an efficient and recyclable heterogeneous catalyst for ketalization. RSC Adv. 4, 12160–12167. https://doi.org/10.1039/C4RA00092G.

Liu, R., Li, T., Xu, J., Zhang, T., Xie, Y., Li, J., Wang, L., 2021. Sandwich-structural Ni/Fe3O4/Ni/cellulose paper with a honeycomb surface for improved absorption performance of electromagnetic interference. Carbohydr. Polym. 260, 117840–117847. https://doi.org/10.1016/j.carbpol.2021.117840.

Liu, G., Yu, S., Hu, W., Qiu, H., 2019. A gold (ɪ)-catalysed three-component reaction via trapping oxonium ylides with allenamides. Chem. Commun. 55, 12675–12678. https://doi.org/10.1039/C9CC06599G.

Loof, D., Hiller, M., Oschkinat, H., Koschek, K., 2016. Quantitative and qualitative analysis of surface modified cellulose utilizing TGA-MS. Materials 9, 415–428. https://doi.org/10.3390/ma9060415.

Magan, R., Marin, C., Salas, J.M., Perez, M.B., Rosales, M.J., 2004. Cytotoxicity of three new triazolo-pyrimidine derivatives against the plant trypanosomatid: phytomonas sp. isolated from euphorbia characias. Men Instaswaldo Cruz, Rio de Janeiro 99, 651–656. https://doi.org/10.1590/S0074-02762004000600021.

Magan, R., Marin, C., Rosales, M.J., Salas, J.M., 2005. Therapeutic potential of new Pt (II) and Ru (III) triazole-pyrimidine complexes against Leishmania donovani. Pharmacology 73, 41–48. https://doi.org/10.1159/000081073.

Maleki, A., Firouzi-Haji, R., Ghassemi, M., Ghafuri, H., 2017. Preparation and application of a magnetic organic-inorganic hybrid nanocatalyst for the synthesis of α-aminonitriles. J. Chem. Sci. 129, 457–462. https://doi.org/10.1007/s12039-017-1253-y.

Maleki, B., Kahoo, G.E., Tayebee, R., 2015. One-pot synthesis of polysubstituted imidazoles catalyzed by an ionic liquid. Org. Prep. Proced. Int. 47, 461–472. https://doi.org/10.1080/00304948.2015.1088757.

Marghaki, N.S., Jonoush, Z.A., Rezaee, A., 2022. Chromium (VI) removal using microbial cellulose/nano-Fe3O4@polypyrrole: Isotherm, kinetic and thermodynamic studies. Mater. Chem. Phys. 278, 125696–125705. https://doi.org/10.1016/j.matchemphys.2022.125696.

Miao, M., Wan, H., Guan, G., 2011a. Synthesis of immobilized Brønsted acidic ionic liquid on silica gel as heterogeneous catalyst for esterification. Catal. Commun. 12, 353–356. https://doi.org/10.1016/j.catcom.2010.10.014.

Miao, J., Wan, H., Shao, Y., Guan, G., Xu, B., 2011b. Acetalization of carbonyl compounds catalyzed by acidic ionic liquid immobilized on silica gel. J. Mol. Catal. A Chem. 348, 77–82. https://doi.org/10.1016/j.molcata.2011.08.005.

Minea, A.A., Sohel Murshed, S.M., 2021. Ionic liquids-based nanocolloids-A review of progress and prospects in convective heat transfer applications. Nanomaterials 11, 1039–1062. https://doi.org/10.3390/nano11041039.

Morais, E.M., Abdurrokhman, I., Martinelli, A., 2022. Solvent-free synthesis of protic ionic liquids. synthesis, characterization and computational studies of triazolium based ionic liquids. J. Mol. Liq. 360, 119358–119391. https://doi.org/10.1016/j.molliq.2022.119358.

Navarro, J.A.R., Salas, J.M., Romero, M.A., Vilaplana, R., Faure, R., 1998. cis-[PtCl2(4,7-H-5-methyl-7-oxo[1,2,4]triazolo[1,5-a]pyrimidine)2]: A sterically restrictive new cisplatin analogue. reaction kinetics with model nucleobases, DNA interaction studies, antitumor activity, and structure-activity relationships. J. Med. Chem. 41, 332–338. https://doi.org/10.1021/jm970358e.

Niknam, K., Deris, A., Naeimi, F., Majleci, F., 2011. Synthesis of 1,2,4,5-tetrasubstituted imidazoles using silica-bonded propylpiperazine N-sulfamic acid as a recyclable solid acid catalyst. Tetrahedron Lett. 52, 4642–4645. https://doi.org/10.1016/j.tetlet.2011.06.105.

Niu, Z., Cheng, W., Cao, M., Wang, D., Wang, Q., Han, J., Long, Y., Han, G., 2021. Recent advances in cellulose-based flexible triboelectric nanogenerators. Nano Energy 87, 106175–106197. https://doi.org/10.1016/j.nanoen.2021.106175.

Oliveira, L.T., Goncalves, R.V., Goncalves, D.V., Azevedo, D.C.S., Pereira de Lucena, S.M., 2019. Superior performance of mesoporous MOF MIL-100 (Fe) impregnated with ionic liquids for CO2 adsorption. J. Chem. Eng. Data. 64, 2221–2228. https://doi.org/10.1021/acs.jced.8b01177.

Patil, P., Yadav, A., Chandam, D., Gurav, R., Hangirgekar, S., Sankpal, S., 2022. [MerDABCO-BSA][HSO4]2: A novel polymer supported Brønsted acidic ionic liquid catalyst for the synthesis of biscoumarins and ortho-aminocarbonitriles. J. Mol. Struct. 1259, 132622–132631. https://doi.org/10.1016/j.molstruc.2022.132622.

Pei, Y., Zhang, Y., Ma, J., Fan, M., Zhang, S., Wang, J., 2022. Ionic liquids for advanced materials. Mater. Today Nano 17, 100159–100182. https://doi.org/10.1016/j.mtnano.2021.100159.

Qiao, K., Hagiwara, H., Yokoyama, C., 2006. Acidic ionic liquid modified silica gel as novel solid catalysts for esterification and nitration reactions. J. Mol. Catal. A Chem. 246, 65–69. https://doi.org/10.1016/j.molcata.2005.07.031.

Rashad, A.E., Hegab, M.I., Abdel-Megeid, R.E., Ali, M.M., Abdel-Megeid, F.M.E., 2010. Synthesis and antitumor evaluation of some

newly synthesized pyrazolopyrimidine and pyrazolotriazolopyrimidine derivatives. Phosphorus Sulfur Silicon Relat. Elem. 185, 74–83. https://doi.org/10.1080/10426500802713267.

Ruijter, E., Orru, R.V., 2013. Multicomponent reactions opportunities for the pharmaceutical industry. Drug Discov. Today Tech. 10, 15–20. https://doi.org/10.1016/j.ddtec.2012.10.012.

Rusinov, V.L., Yu-Petrov, A., Pilicheva, T.L., Chupakhin, O.N., Kovalev, G.V., Komina, E.R., 1986. Synthesis and study of cardiovascular activity of 6-nitro-7-oxo-4,7-dihydroazolo[1,5-a]pyrimidine derivatives. Pharm. Chem. J. 20, 113–117. https://doi.org/10.1007/BF00766904.

Sabaqian, S., Nemati, F., Taherpour-Nahzomi, H., Heravi, M.M., 2017. Silver (I) dithiocarbamate on modified magnetic cellulose: Synthesis, density functional theory study and application. J. Carbohydr. Polym. 184, 221–230. https://doi.org/10.1016/j.carbpol.2017.12.045.

Sadeghzadeh, S.M., Daneshfar, F., Malekzadeh, M., 2014. Manganese (III) salen complex immobilized on Fe_3O_4 magnetic nanoparticles: the efficient, green and reusable nanocatalyst. Chin. J. Chem. 32, 349–355. https://doi.org/10.1002/cjoc.201400007.

Saeedi, S., Rahmati, A., 2022. MNP-cellulose-OSO_3H as an efficient and biodegradable heterogeneous catalyst for green synthesis of trisubstituted imidazoles. RSC Adv. 12, 11740–11749. https://doi.org/10.1039/d2ra01348g.

Safari, J., Ahmadzadeh, M., 2017. Zwitterionic sulfamic acid functionalized nanoclay: A novel nanocatalyst for the synthesis of dihydropyrano[2,3-c]pyrazoles and spiro[indoline-3,4-pyrano[2,3-c]pyrazole] derivatives. J. Taiwan Inst. Chem. Eng. 74, 14–24. https://doi.org/10.1016/j.jtice.2016.12.010.

Shang, Q., Liu, C., Hu, Y., Jia, P., Hu, L., Zhou, Y., 2018. Bio-inspired hydrophobic modification of cellulose nanocrystals with castor oil. Carbohydr. Polym. 191, 168–175. https://doi.org/10.1016/j.carbpol.2018.03.012.

Sheykhan, M., Mamani, L., Ebrahimi, A., Heydari, A., 2011. Sulfamic acid heterogenized on hydroxyapatite-encapsulated γ-Fe2O3 nanoparticles as a magnetic green interphase catalyst. J. Mol. Catal. A: Chem. 335, 253–261. https://doi.org/10.1016/j.molcata.2010.12.004.

Singh, S.K., Savoy, A.W., 2020. Ionic liquids synthesis and applications: An overview. J. Mol. Liq. 297, 112038–112101. https://doi.org/10.1016/j.molliq.2019.112038.

Singh, P.K., Choudhary, S., Kashyap, A., Verma, H., Kapil, S., Kumar, M., Arora, M., Silakari, O., 2019. An exhaustive compilation on chemistry of triazolopyrimidine: A journey through decades. Bioorg. Chem. 88, 102919–102942. https://doi.org/10.1016/j.bioorg.2019.102919.

Slobbe, S., Ruijter, E., Orru, R.V.A., 2012. Recent applications of multicomponent reactions in medicinal chemistry. Med. Chem. Commun. 3, 1189–1218. https://doi.org/10.1039/C2MD20089A.

Sun, Q., Aguila, B., Perman, J., Earl, L.D., Abney, C.W., Cheng, Y., Wei, H., Nguyen, N., Wojtas, L., Ma, S., 2017. Postsynthetically modified covalent organic frameworks for efficient and effective mercury removal. J. Am. Chem. Soc. 139, 2786–2793. https://doi.org/10.1021/jacs.6b12885.

Sunderhaus, J.D., Martin, S.F., 2009. Applications of multicomponent reactions to the synthesis of diverse heterocyclic scaffolds. Chemistry 15, 1300–1308. https://doi.org/10.1002/chem.200802140.

Tabrizian, E., Amoozadeh, A., Rahmani, S., 2016. Sulfamic acid-functionalized nano-titanium dioxide as an efficient, mild and highly recyclable solid acid nanocatalyst for chemoselective oxidation of sulfides and thiols. RSC Adv. 6, 21854–21864. https://doi.org/10.1039/C5RA20507G.

Tajbakhsh, M., Alinezhad, H., Norouzi, M., Baghery, S., Akbari, M., 2013. Protic pyridinium ionic liquid as a green and highly efficient catalyst for the synthesis of polyhydroquinoline derivatives via Hantzsch condensation in water. J. Mol. Liq. 177, 44–48. https://doi.org/10.1016/j.molliq.2012.09.017.

Tayebee, R., Jomei, M., Maleki, B., Razi, M.K., Veisi, H., Bakherad, M., 2015. A new natural based ionic liquid 3-sulfonic acid 1-imidazolopyridinium hydrogen sulfate as an efficient catalyst for the preparation of 2H-indazolo[2,1-b]phthalazine-1,6,11(13H)-triones. J. Mol. Liq. 206, 119–128. https://doi.org/10.1016/j.molliq.2015.02.021.

Tayebee, R., Abdizadeh, M.F., Maleki, B., Shahri, E., 2017. Heteropolyacid-based ionic liquid $[Simp]_3PW_{12}O_{40}$ nanoparticle as a productive catalyst for the one-pot synthesis of 2H-indazolo [2,1-b] phthalazine-triones under solvent-free conditions. J. Mol. Liq. 241, 447–455. https://doi.org/10.1016/j.molliq.2017.06.033.

Testa, M.L., La Parola, V., Venezia, A.M., 2010. Esterification of acetic acid with butanol over sulfonic acid-functionalized hybrid silicas. Catal. Today 158, 109–113. https://doi.org/10.1016/j.cattod.2010.05.027.

Traxler, P.M., Furet, P., Mett, H., Buchdunger, E., Meyer, T., Lydon, N., 1996. 4-(Phenylamino)pyrrolopyrimidines: Potent and Selective, ATP Site Directed Inhibitors of the EGF-Receptor Protein Tyrosine Kinase. J. Med. Chem. 39, 2285–2292. https://doi.org/10.1021/jm960118j.

Váradi, A., Palmer, T.C., Dardashti, R.N., Majumdar, S.J., 2016. Isocyanide-based multicomponent reactions for the synthesis of heterocycles. Molecules 21, 19–40. https://doi.org/10.3390/molecules21010019.

Veisi, H., Karmakar, B., Tamoradi, T., Tayebee, R., Sajjadifar, S., Lotfi, S., Maleki, B., Hemmati, S., 2021. Bio-inspired synthesis of palladium nanoparticles fabricated magnetic Fe_3O_4 nanocomposite over Fritillaria imperialis flower extract as an efficient recyclable catalyst for the reduction of nitroarenes. Scientific Reports 11, 1–15. https://doi.org/10.1038/s41598-021-83854-1.

Wang, Q., Zhang, S., Yu, Y., Dai, B., 2020. High-performance of plasma-enhanced Zn/MCM-41 catalyst for acetylene hydration. Catal. Commun. 147, 106122–106142. https://doi.org/10.1016/j.catcom.2020.106122.

Wei, Z., Abbaspour, S., Tayebee, R., 2021. Nickel nanoparticles originated from cressa leafextract in the preparation of a novel Melem@Ni-HPA photocatalyst for the synthesis of some chromenes and a preliminary MTT assay on the anticancer activity of the nanocomposite. Polycycl. Aromat. Compd 1–20. https://doi.org/10.1080/10406638.2021.2019063.

Wu, J., Kozak, J.A., Simeon, F., Hatton, T.A., Jamison, T.F., 2014. Mechanism-guided design of flow systems for multicomponent reactions: conversion of CO_2 and olefins to cyclic carbonates. Chem. Sci. 5, 1227–1231. https://doi.org/10.1039/C3SC53422G.

Zaharani, L., Ghaffari-Khaligh, N., Mihankhah, T., Johan, M.R., Hamizi, N.A., 2020. Facile and green synthesis of a series of dihydro-[1,2,4]triazolo[1,5-a]pyrimidine scaffolds. Canad. J. Chem. 98, 630–634. https://doi.org/10.1139/cjc-2020-0145.

Zareai, Z., Khoobi, M., Ramazani, A., Foroumadi, A., Souldozi, A., Slepokura, K., Lis, T., Shafiee, A., 2012. Synthesis of functionalized furo[3,2-c]coumarins via a one-pot oxidative pseudo three-component reaction in poly(ethylene glycol). Tetrahedron 68, 6721–6726. https://doi.org/10.1016/j.tet.2012.05.112.

Zhang, H., Li, H., Pan, H., Wang, A., Souzanchi, S., Xu, C., Yang, S., 2018. Magnetically recyclable acidic polymeric ionic liquids decorated with hydrophobic regulators as highly efficient and stable catalysts for biodiesel production. Appl. Energy 223, 416–429. https://doi.org/10.1016/j.apenergy.2018.04.061.

Zhang, Y., Li, J., Ma, N., Meng, Z., Sui, G., 2019. Processing cellulose@Fe_3O_4 into mechanical, magnetic and biodegradable synapse-like material. Compos. B. 177, 107432–107440. https://doi.org/10.1016/j.compositesb.2019.107432.

Zhang, Q., Su, H., Luo, J., Wei, Y., 2012a. A magnetic nanoparticle supported dual acidic ionic liquid: a quasi-homogeneous catalyst for the one-pot synthesis of benzoxanthenes. Green Chem. 14, 201–208. https://doi.org/10.1039/C1GC16031A.

Zhang, Q., Su, H., Luo, J., We, Y., 2012b. A magnetic nanoparticle supported dual acidic ionic liquid: a quasi-homogeneous catalyst

for the one-pot synthesis of benzoxanthenes. Green Chem. 14, 201–208. https://doi.org/10.1039/C1GC16031A.

Zhi, S., Ma, X., Zhang, W., 2019. Consecutive multicomponent reactions for the synthesis of complex molecules. Org. Biomol. Chem. 17, 7632–7650. https://doi.org/10.1039/C9OB00772E.

Zolfigol, M.A., Ayazi-Nasrabadi, R., Baghery, S., Khakyzadeh, V., Azizian, S., 2016. Applications of a novel nano magnetic catalyst in the synthesis of 1,8-dioxo-octahydroxanthene and dihydropyrano [2,3-c]pyrazole derivatives. J. Mol. Catal. A: Chem. 418, 54–67. https://doi.org/10.1016/j.molcata.2016.03.027.